

DOI: 10.1002/((please add manuscript number))

Article type: Communication

Enhanced ferroelectric property of P(VDF-TrFE-CTFE) film using room temperature crystallization for high performance ferroelectric device applications

Yuljae Cho^a, Docheon Ahn^a, Jong Bae Park, Sangyeon Pak, Sanghyo Lee, Byoung Ok Jun, John Hong, Su Yong Lee, Jae Eun Jang, Jinpyo Hong, Stephen M. Morris, Jung Inn Sohn*, SeungNam Cha*, and Jong Min Kim

Mr. Yuljae Cho, Dr. Sanghyo Lee, Mr. Sangyeon Pak, Mr. John Hong, Prof. Stephen M. Morris, Dr. Jung Inn Sohn, Prof. SeungNam Cha
Department of Engineering Science, University of Oxford
Parks Road, Oxford, OX1 3PJ, United Kingdom
E-mail: seungnam.cha@eng.ox.ac.uk, junginn.sohn@eng.ox.ac.uk

Dr. Docheon Ahn, Dr. Su Yong Lee
Beamline Department, Pohang Accelerator Laboratory (PAL), Pohang 790-784, Republic of Korea

Dr. Jong Bae Park
Jeonju Center, Korea Basic Science Institute, Jeonju, Jeollabuk-do 54907, Republic of Korea

Mr. Byoung Ok Jun, Prof. Jae Eun Jang
Department of Information and Communication Engineering, Daegu Gyeongbuk Institute of Science and Technology, Daegu 711-873, Republic of Korea

Prof. Jinpyo Hong
Department of Physics, Hanyang University, Seoul 133-791, Republic of Korea

Prof. Jong Min Kim
Department of Engineering, University of Cambridge, 9 JJ Thomson Avenue, Cambridge CB3 0FA, UK

^aThese authors contributed equally to this work

Keywords: ferroelectric polymers, ferroelectric phase, paraelectric phase, phase transition, solvent annealing, P(VDF-TrFE-CTFE)

Ferroelectric polymers have attracted considerable interest in the scientific research community as a result of their potential in next-generation electronics and energy applications. This interest stems from a set of attractive characteristics, such as flexibility, ease of processing, cost-effectiveness, and environmentally-friendly nature. Furthermore, the ferroelectric properties of these polymers are often comparable to that of their inorganic counterparts.^[1-8] In recent years, polyvinylidene fluoride (PVDF)-based polymers have elicited much attention because of the potential technological benefits including large spontaneous polarization and excellent polarization stability.^[5,6,7] Among the various PVDF-based polymers, the class of terpolymers have shown significantly improved inherent dielectric constant (κ) and electromechanical properties, which are necessary requirements for electronic and energy applications.^[9-12] In particular, poly(vinylidene fluoride-trifluoroethylene-chlorotrifluoroethylene) (P(VDF-TrFE-CTFE)) is considered to be one of the promising materials as it has a higher polarization, which is one of the most important characteristics of a ferroelectric polymer. It is attributed to the chlorine atoms in the third monomer CTFE that imposes a large steric hindrance, facilitating the formation of trans conformation.^{[9][13]} Additionally, it has been reported that P(VDF-TrFE-CTFE) has a much higher dielectric constant (κ) than other PVDF-based polymers as well as a high electromechanical response and elastic energy density. As a result, the combination of the properties of P(VDF-TrFE-CTFE) are particularly promising in the development of a range of devices that exhibit a highly efficient electromechanical performance as well as a lack of degradation arising from dielectric leakage.^[14-20]

Notwithstanding these attractive features and potential benefits, however, there still remain a number of important challenges that are associated with the formation of the ferroelectric phase in the P(VDF-TrFE-CTFE) polymer. This is an essential requirement for ferroelectric devices such as ferroelectric field effect transistors (feFET) and mechanical energy harvesting devices.^[1,2,7,8] Several reports have revealed that a paraelectric α phase is

stable and dominant above the ferroelectric to paraelectric (F-P) transition temperature, i.e. Curie temperature (T_c), due to an irreversible phase transition behaviour, which severely causes the ferroelectricity to fade, resulting in the deterioration of the device performance.^[11,17,21] As a result, despite the remarkable features of the P(VDF-TrFE-CTFE) polymer it has not received as much attention as an active material in ferroelectric devices compared with other PVDF-based polymers. It is therefore necessary to seek a facile, reproducible, and low-temperature approach to forming the ferroelectric phase through a deeper understanding of the phase transition mechanism.

In this work, we introduce a room temperature annealing method, referred to as solvent annealing, to form the ferroelectric β phase in a P(VDF-TrFE-CTFE) film by crystallizing the polymer below the F-P transition temperature while avoiding the routinely employed thermal annealing method. Using a solvent annealing method, it was possible to form a ferroelectric β phase-dominant film that showed significantly enhanced ferroelectricity compared to a thermally annealed one. In addition, studies on the F-P transition through *in-situ* x-ray diffraction (XRD) and differential scanning calorimeter (DSC) gave insight into the phase transition mechanism in P(VDF-TrFE-CTFE). These measurements formed the basis on which we demonstrate a ferroelectric polymer P(VDF-TrFE-CTFE) as a promising active material for feFET and energy harvesting devices by showing outstanding device performances, which are attributed to the enhanced ferroelectric and materials properties.

Figure 1 describes two different annealing processes in order to crystallize a P(VDF-TrFE-CTFE) polymer film. Annealing a P(VDF-TrFE-CTFE) polymer film above the F-P transition temperature is known to thermodynamically stabilize the paraelectric α -phase. Therefore, in order to attain a ferroelectric β -phase polymer film, a new annealing method that is performed below the F-P transition is required. Compared to the conventional process of thermal annealing (TA), a room temperature annealing method, solvent annealing (SA),^[22,23] was applied to a spin-coated polymer film in order to avoid crystallizing the material above

the F-P transition temperature. All annealing methods were carried out using an identical spin-coating procedure. Following the different annealing processes, each film formed different phases. For the TA method it was found that the film was dominated by the paraelectric α -phase whereas for the SA process the ferroelectric β -phase was formed in the film. As shown in Figure 1, each phase is depicted by a different molecular structure and this results in different net dipole moments in the polymer film. For the ferroelectric β -phase, electric dipoles are formed vertically with a unidirectional orientation, thereby increasing the net surface normal dipole moments of the film. In contrast, for the paraelectric α -phase the net surface normal dipole moments is almost zero as the electric dipoles are formed horizontally.

The formation of the different phases for the TA and SA treated films were measured and compared using XRD measurements as shown in Figure 2(a). A TA film showed a sharp XRD peak at 18.4° , which is associated with the paraelectric α -phase.^[17,21] In contrast, an SA treated film revealed right shifted XRD peak toward 19.4° that is attributed to the formation of the ferroelectric β -phase.^[17,24,25] A relatively broad SA peak might be due to either the existence of a small portion of the α -phase or weak long-range ordering.^[17] Consistent with XRD measurements, DSC analysis revealed that P(VDF-TrFE-CTFE) films prepared through different annealing methods did indeed lead to the formation of different phases. As shown in Figure 2(b), each film showed noticeably different aspects during the first cycle of the analysis. An SA film showed the first endotherm in the temperature range 38.8 to 45.5°C , which is referred to as the F-P transition point and the second endotherm that is related to the melting point,^[11,26] suggesting that the SA film was in the ferroelectric phase at first before changing to the paraelectric phase during the heating cycle. In contrast, only a melting endotherm was observed without any noticeable endotherm related to the phase transition in a TA film. The second small endotherm is thought to be associated with a small fraction of another phase, gamma or delta,^[9] which means that the TA film consists of the paraelectric-

dominant phase. The results are summarized in Supplementary Table 1 and three cycles of DSC graphs are shown in Supplementary Figure S1.

To further understand the phase transition mechanism, an investigation on the F-P phase transition was performed using *in-situ* XRD measurements. An SA film was heated and cooled down subsequently in ambient air at a heating rate of 10 °C per minute and a cooling rate of 5 °C per minute, respectively. Details of the *in-situ* XRD measurement procedure are explained in the Supplementary information. As shown in Figures 2(c) and (d), a phase transition from the ferroelectric to paraelectric phase was observed in the temperature range of 35 to 45 °C during the heating cycle. A minor phase shift was observed above a temperature of 45 °C, which is due to an uncompleted phase transition and the thermal expansion of the polymer molecules at high temperature.^[27] Above 90 °C, there was no further shift as there was no subsequent thermal expansion of the polymer molecules. Conversely, the XRD peak was found to shift to the right as the polymer molecules relaxed to their normal states as the temperature decreased during the cooling cycle, which is shown in Figure 2(d). It is noteworthy that irreversible phase transition behaviour was observed during the cooling cycle as the XRD peak remained at the shifted position, approximately 18.4 °. The XRD measurement result is consistent with the DSC analysis that demonstrated an SA film had only a melting endotherm after the first heating cycle as shown in Supplementary Figure S1, indicating that the phase transition is irreversible. Through crystallographic and thermochemical analysis, it was demonstrated that a ferroelectric phase was only formed by an SA method and the mechanism responsible for the phase transition was irreversible.

To further support the formation of a ferroelectric phase in the SA film that was prepared through a solvent annealing method, we conducted atomic force microscopy (AFM) and piezo force microscopy (PFM). Details of the PFM measurement are provided in the Supplementary Information. Figures 3(a) and (b) show the surface morphology of the SA and TA films,

respectively. A root-mean-square roughness was calculated for each film and was found to exhibit almost the same roughness, approximately 1.7 nm over an area of 4 by 4 μm^2 . A 10 V DC bias was applied to a conducting tip with a size of 1 by 1 μm^2 area on each SA and TA film. Right after the poling process by the PFM tip, the amplitude and phase were read by applying a 2 V AC bias to the tip with a size of 2 by 2 μm^2 area. Due to the polarization of the electric dipoles in the film by electrical poling, there was a clear difference in the PFM amplitude and phase between a poled and an unpoled region for the SA film. In contrast, for a TA film no detectable piezoelectric response was observed between the two regions as shown in Figures 3(c) and (d). In addition, the contrast for the electrically poled region in the SA film was maintained for more than 150 minutes, which is comparable to the representative inorganic ferroelectric material BaTiO_3 .^[28] A TA film, on the other hand, showed relatively fast relaxation of the dipoles on a timescale of 40 minutes. The long-time retention of the polarization in the SA film was due to the presence of the permanent electric dipoles in the ferroelectric phase in the absence of an external electric field, which supports the evidence of the formation of a ferroelectric β phase in the SA film. On the contrary, weak and short-time piezo response on a TA film indicates that the film is not ferroelectric but rather paraelectric given that electric dipoles in the film responded only when an external electrical field was applied. PFM measurements, therefore, revealed that the SA film is in the ferroelectric-dominant phase as the polarization of the electric dipoles in the film were retained at least 4 times longer than that of a TA film.

As the ferroelectric β phase consists of electric dipoles which show spontaneous polarization due to a preferential direction, the surface properties of the β -phase and the α -phase films were subsequently different. Surface potential provides useful information for demonstrating the electrical properties of the surface that are induced by electric charges and/or dipoles.^[23,29] As revealed by surface potential measurements in Figure 4(a), the SA film showed more than two times higher surface potential than that of the TA film, which is

attributed to electric dipoles in the SA film. Surface potential in the TA film is due to a small portion of other phases such as the gamma or delta being present in the film as well as electrostatic charges. Enhanced ferroelectric properties in the SA film revealed by PFM and surface potential measurements are desirable for non-volatile memory and mechanical energy harvesting devices as the stability and performance of devices depend on the ferroelectric properties of the film.^[1,2,7,8] It was demonstrated that an SA film employed memory device (SAMD) showed improved durability, reliability, and retention time compared to that of a TA film employed memory device (TAMD). All memory devices were measured using a back gate contact. Details of the fabrication methods used for the memory devices and the measurement procedure are provided in the experimental section. A memory device before P(VDF-TrFE-CTFE) deposition showed threshold voltages around -10 V at $V_{ds} = 1$ V swept from $-40 \sim 40$ V gate voltage. Due to the spontaneous polarization of the electric dipoles in an SA film, a shift of the threshold voltage was observed after P(VDF-TrFE-CTFE) deposition on the indium gallium zinc oxide (IGZO) channel as shown in Figure 4(b). The thickness of the P(VDF-TrFE-CTFE) (4 wt%) film was approximately 500 nm measured by DEKTAK. Thickness information for other concentrated solution is shown in Supplementary Information. In the figure, the grey curve shows a transfer curve of before P(VDF-TrFE-CTFE) deposition and a black curve shows after P(VDF-TrFE-CTFE) deposition. Supplementary Figure S2(a) describes an accumulated and a depleted channel mode with respect to the direction of electric dipoles, which were controlled by switching the dipoles through an electrical poling process. Details of the electrical poling process are described in experimental section. As shown in Figure 4(b), a shift of the transfer curve, i.e. threshold voltage (V_{th}), at each mode was noticeably large after a poling process. The extent of the shift was different for each mode with respect to the reference curve which is depicted as a black transfer curve measured without switching the electric dipoles in Figure 4(b). This is because the electric dipoles have a spontaneous polarization to the preferential direction.^[30-32] As a

result, the right shift is more prominent than the left shift of the transfer curve. Device parameters and characteristics of the SAMD were listed in Supplementary Tables 2 and 3. Hysteresis in the devices was investigated in order to prove that the shift of the threshold voltage was due to a ferroelectric effect of the SA film and was not from the IGZO channel. Supplementary Figure S3 shows clearly that in the range of gate voltage -40 to 40 V where all device measurements were performed, the hysteresis was negligible for memory devices, indicating that the shift of V_{th} was due to electric dipole switching in the ferroelectric β -phase SA film and on and off states were not affected by hysteresis effect. As shown in Figure 4(c), memory retention time was measured and turned out to be stable for 2700 seconds (45 minutes) while maintaining 10^5 order. A stark contrast was observed with the TAMd. As shown in Supplementary Figure S2(c), the retention time was found to be on the order of 700 seconds, which was less than one third of that of the SAMD. This is because a TA film is paraelectric and thus electric dipoles exhibit a temporary polarization and relaxed quickly without the application of external electrical field. A large shift of the threshold voltage and the significantly enhanced retention time for the SAMD compared to that of the TAMd are attributed to the electric dipoles in the ferroelectric phase in the SA film, indicating the formation of ferroelectric dominant phase through the solvent annealing method, which is consistent with the in-situ XRD, DSC and PFM results.

Another emerging area where ferroelectric polymers are in high demand is energy harvesting that generates electricity from wasted mechanical vibration energy.^[23,30,33] A certain surface polarity and higher surface charge density induced by electric dipoles are important factors for attaining higher electrical energy, which means higher surface potential on an SA film can generate more electrical energy than a TA film. As shown in Figures 4(d) and (e), an SA film employed energy generator (SEG) produced more than four times higher potential and current density than those of a TA film employed energy generator (TEG), around 230 V and $23 \mu\text{A cm}^{-2}$ for SEG while 60 V and $6 \mu\text{A cm}^{-2}$ for TEG. All measurements

were performed at an input frequency of 3 Hz with a pressure of 2 N cm^{-2} by the pressure stamping machine. As shown in Supplementary Figure S4, the potential and current density of the SEG were largely the result of the triboelectric effect/charge that was strengthened by electric dipoles in the ferroelectric β -phase film (Figure 4(a)), although a minor contribution did appear to come from the piezoelectric effect. Harvested energy from the SEG and TEG was respectively more than 20 times and 5 times higher than those from P(VDF-TrFE) based energy harvesters in our previous work,^[23] which is attributed to the inherently high electromechanical response, elastic energy density and a higher dielectric constant in P(VDF-TrFE-CTFE).^[14-18] The asymmetry in the characteristics of the voltage and current density were due to the differences in the application and removal speeds of the pressure that was applied to the energy generator and is a common feature that has been observed in other energy harvesters.^[30,34-36] The maximum power density obtained by the SEG was approximately 2.8 mW cm^{-2} at a load of $9 \text{ M}\Omega$ as shown in Supplementary Figure S5(a). To further evaluate the performances of the SEG and TEG, the capacitor charging rate of the SEG and TEG were compared. As shown in Figure 4(f), the charging rates of the capacitor were noticeably different from each other. In 240 seconds, the TEG charged the $110 \text{ }\mu\text{F}$ capacitor to 1.1 V whereas the SEG charged the same capacitors to 10 V, which is almost ten times higher than that of TEG. The before and after rectifying potentials generated by each TEG and SEG are shown in Supplementary Figure S6. In order to increase the charge generation rates, the SEG was driven at a higher frequencies ranging from 1 to 50 Hz by pressure stamping machine. Within a certain period, the energy density generated by the SEG was optimized by the vibration frequency and the maximum output was attained at a frequency of 30 Hz (Supplementary Figure S5(b) and (c)). Insets in Figure 4(f) show a relay controller circuit connected to an energy harvesting device (left) and 6 blue LEDs turned on by the energy generator driven at 30 Hz. The generated energy was rectified by a bridge circuit and charged a series of $10 \text{ }\mu\text{F}$ capacitors. For every 0.5 seconds, the switch was turned

on for 0.1 second and then turned off as shown in Supplementary Video 1. The LEDs were bright enough to be seen by the naked eye when the lights were on.

In summary, the ferroelectric β -phase in P(VDF-TrFE-CTFE) was successfully formed using a room temperature annealing process, referred to as the solvent annealing method, which was not possible using the conventional thermal annealing method as the P(VDF-TrFE-CTFE) polymer shows an irreversible phase transition behaviour. Through *in-situ* XRD and DSC analysis, the F-P phase transition mechanism was studied and PFM measurements showed enhanced ferroelectricity in a solvent annealed film compared to a thermally annealed film. Finally, applications in electronics and energy, where ferroelectric properties are highly required, were demonstrated. Significantly enhanced device performances for an SA film employed devices compared to a TA film employed ones were attributed to the formation of the ferroelectric β phase and the inherent material properties.

Experimental section.

P(VDF-TrFE-CTFE) powder (PVDF:TrFE:CTFE = 62:31:7 in Mole %) was purchased from PIEZOTECH ARKEMA and dissolved in 2-Butanone (ACS reagent, $\geq 99\%$, Sigma Aldrich) at a concentration of 2 ~ 10 wt%. The solution was stirred for one day at room temperature and then stirred for one to two hours before it was used.

Sample preparation

P(VDF-TrFE-CTFE) solution was spin-coated at 500 rpm for 10 seconds and then 3000 rpm for 40 seconds on a substrate. Thermal annealing was performed in oven in ambient atmosphere at 130 °C for 2 hours. For the solvent annealing process, samples were placed on a sample holder in a closed chamber with 2-Butanone underneath the sample holder. Solvent annealing was applied to the film for 30 min per 1 μm right after spin-coating. Solvent annealing method crystallizes P(VDF-TrFE-CTFE) films slowly and consequently prevents polymers from losing their crystallinity which is caused by such as fast evaporation of the

solvent during thermal annealing process [37,38,39]. Then, the samples were dried in the vacuum chamber for 10 hours to remove the solvent from inside of the film. The dielectric constant of the (PVDF-TrFE-CTFE) that was measured by the material supplier (PIEZOTECH ARKEMA) was found to be 30 (obtained from capacitance measurement at 1 kHz) whereas the remnant polarization was $0.75 \mu\text{C cm}^{-2}$ (at 1 kHz) for the SA film, which is comparable to that of previously reported PVDF-based ferroelectric polymers [40].

Device Characterization.

1. FET devices Fabrication.

SiO₂ substrates with 200 nm-thick dielectric layers were used for the fabrication of the FET devices. The semiconducting channel material, α -IGZO (InGaZnO₄), with 50 nm thickness was sputtered by the RF magnetron sputtering system at a gas mixing ratio of argon 50 to O₂ 5 sccm at an input power of 400 W and a pressure of 5 mTorr. Then, with a photolithography process, α -IGZO was patterned and wet-etched by a buffered oxide etchant (BOE) and thermally annealed in oxygen ambient environment at 300 °C for one hour. Finally, source and drain electrodes were patterned by a photolithography process and aluminum sources were sputtered by a DC magnetron with a gas mixing ratio of Ar 120 to O₂ 5 sccm at an input voltage of 400 V and a pressure of 5 mTorr. The thickness of source and drain electrodes was 100 nm [41].

2. FET measurement.

IGZO was used as a semiconducting channel material. Channel width and length were 5 and 8 μm , respectively. All measurements were performed by back gate contact at 1 V drain-source voltage. 4 wt% P(VDF-TrFE-CTFE) solution was spin-coated on the channel and the thickness of a P(VDF-TrFE-CTFE) film was 500 nm. Electrical poling was performed so as to switch the electric dipoles of the P(VDF-TrFE-CTFE) film by applying 80 V for positive poling and -80 V for negative poling for 30 seconds to the gate electrode and zero voltage to

the moveable counter electrode that was positioned on to the channel. Retention time was measured at 1 V drain-source and 0 V gate voltage.

3. *Energy harvesting devices.*

Surface potential was measured by an electrostatic voltmeter (TREK 542A) at the same conditions to minimize measurement errors. Flexible Indium oxide electrodes purchased from Sigma Aldrich (surface resistivity $\leq 10 \Omega \text{ sq}^{-1}$) were used for both bottom and top electrodes. 10 wt% CTFE solution was used for making energy harvesting devices with a spacer, approximately 0.17 mm thick, between a P(VDF-TrFE-CTFE) film and a top electrode. The size of the samples was 3 by 3 cm and the active area was 2.25 cm^2 . Potential and current were measured by an oscilloscope (Lecroy) and a current amplifier (Stanford).

Acknowledgements

This work was supported by the International Collaborative Energy Technology R&D Program of the Korea Institute of Energy Technology Evaluation and Planning (KETEP), granted financial resource from the Ministry of Trade, Industry & Energy, Republic of Korea (20142020103970). The research leading to these results has received funding from the European Union's Seventh Framework Programme (FP7/2007-2013) under grant agreement number (611887) and European Commission Horizon2020 under grant agreement number (685758).

Received: ((will be filled in by the editorial staff))

Revised: ((will be filled in by the editorial staff))

Published online: ((will be filled in by the editorial staff))

[1] R. C. Naber, C. Tanase, P. W. Blom, G. H. Gelinck, A. W. Marsman, F. J. Touwslager, S. Setayesh, D. M. De Leeuw, *Nat. Mater.* **2005**, 4, 243.

[2] K. Asadi, D. M. De Leeuw, B. De Boer, P. W. Blom, *Nat. Mater.* **2008**, 7, 547.

- [3] S. Cha, S. M. Kim, H. Kim, J. Ku, J. I. Sohn, Y. J. Park, B. G. Song, M. H. Jung, E. K. Lee, B. L. Choi, *Nano lett.* **2011**, 11, 5142.
- [4] Q. Sun, W. Seung, B. J. Kim, S. Seo, S. Kim, J. H. Cho, *Adv. Mater.* **2015**, 27, 3411.
- [5] R. C. Naber, C. Tanase, P. W. Blom, G. H. Gelinck, A. W. Marsman, F. J. Touwslager, S. Setayesh, D. M. De Leeuw, *Nat. Mater.* **2005**, 4, 243.
- [6] Z. Hu, M. Tian, B. Nysten, A. M. Jonas, *Nat. Mater.* **2009**, 8, 62.
- [7] R. H. Kim, H. J. Kim, I. Bae, S. K. Hwang, D. B. Velusamy, S. M. Cho, K. Takaishi, T. Muto, D. Hashizume, M. Uchiyama, *Nat. Commun.* **2014**, 5, 3583.
- [8] L. Persano, C. Dagdeviren, Y. Su, Y. Zhang, S. Girardo, D. Pisignano, Y. Huang, J. A. Rogers, , *Nat. Commun.* **2013**, 4, 1633.
- [9] G. Buckley, C. Roland, R. Casalini, A. Petchsuk, T. Chung, *Chem. Mat.* **2002**, 14, 2590.
- [10] H. Xu, Z. Cheng, D. Olson, T. Mai, Q. Zhang, G. Kavarnos, *Appl. Phys. Lett.* **2001**, 78, 2360
- [11] Y. Lu, J. Claude, B. Neese, Q. Zhang, Q. Wang, *J. Am. Chem. Soc.* **2006**, 128, 8120.
- [12] X. Chen, L. Liu, S. Liu, Y. Cui, X. Chen, H. Ge, Q. Shen, *Appl. Phys. Lett.* **2013**, 102, 063103.
- [13] G. J. Kavarnos, R. Holman, *Polymer* **1994**, 35, 5586.
- [14] F. Xia, Z. Cheng, H. Xu, H. Li, Q. Zhang, G. J. Kavarnos, R. Y. Ting, G. Abdul-Sadek, K. D. Belfield, *Adv. Mater.* **2002**, 14, 1574.
- [15] F. Bauer, *IEEE Trans. Dielectr. Electr. Insul.* **2010**, 17, 1106.
- [16] K. Ren, Y. Liu, H. Hofmann, Q. Zhang, J. Blottman, *Appl. Phys. Lett.* **2007**, 91, 132910.
- [17] O. L. Smith, Y. Kim, M. Kathaperumal, M. R. Gadinski, M. Pan, Q. Wang, J. W. Perry, *ACS Appl. Mater. Inter.* **2014**, 6, 9584.
- [18] S. K. Hwang, I. Bae, S. M. Cho, R. H. Kim, H. J. Jung, C. Park, *Adv. Funct. Mater.* **2013**, 23, 5484.
- [19] A. I. Kingon, J. Maria, S. Streiffer, *Nature* **2000**, 406, 1032.

- [20] A. Facchetti, M. Yoon, T. J. Marks, *Adv. Mater.* **2005**, 17, 1705.
- [21] H. Li, K. Tan, Z. Hao, G. He, *J. Appl. Polym. Sci.* **2011**, 122, 3007.
- [22] S. H. Kim, M. J. Misner, T. Xu, M. Kimura, T. P. Russell, *Adv. Mater.* **2004**, 16, 226.
- [23] Y. Cho, J. B. Park, B. Kim, J. Lee, W. Hong, I. Park, J. E. Jang, J. I. Sohn, S. Cha, J. M. Kim, *Nano Energy*. **2015**, 16, 524.
- [24] H. Gong, B. Miao, X. Zhang, J. Lu, Z. Zhang, *RSC Adv.* **2016**, 6, 1589.
- [25] Z. Li, J. Wang, X. Wang, Q. Yang, Z. Zhang, *RSC Adv.* **2015**, 5, 80950.
- [26] R. J. Klein, F. Xia, Q. Zhang, F. Bauer, *J. Appl. Phys.* **2005**, 97, 094105.
- [27] Y. Hsieh, X. Hu, *J. Polym. Sci. Pol. Phys.* **1997**, 35, 623.
- [28] Z. Wen, C. Li, D. Wu, A. Li, N. Ming, *Nat. Mater.* **2013**, 12, 617.
- [29] S. Wang, Y. Zi, Y.S. Zhou, S. Li, F. Fan, L. Lin, Z.L. Wang, *J. Mater. Chem. A* **2016**, 4, 3728.
- [30] J. Lee, R. Hinchet, T. Y. Kim, H. Ryu, W. Seung, H. Yoon, S. Kim, *Adv. Mater.* **2015**, 27, 5553.
- [31] B. Li, C. Xu, F. Zhang, J. Zheng, C. Xu, *J. Mater. Chem. C* **2015**, 3, 8926.
- [32] S. Maji, P. K. Sarkar, L. Aggarwal, S. K. Ghosh, D. Mandal, G. Sheet, S. Acharya, *Phys. Chem. Chem. Phys.* **2015**, 17, 8159.
- [33] F.R. Fan, W. Tang, Z.L. Wang, *Adv. Mater.* **2016**, 28, 4283.
- [34] J.-H. Lee, H.-J. Yoon, T.Y. Kim, M.K. Gupta, J.H. Lee, W. Seung, H. Ryu, S.-W. Kim, *Adv. Funct. Mater.* **2015**, 25, 3203.
- [35] J. Chun, J. W. Kim, W.-S. Jung, C.-Y. Kang, S.-W. Kim, Z. L. Wang, J. M. Baik, *Energy Environ. Sci.* **2015**, 8, 3006.
- [36] J. -H. Lee, R. Hinchet, S. K. Kim, S. Kim, S.-W. Kim, *Energy Environ. Sci.* **2015**, 8, 3605.
- [37] G. Li, Y. Yao, H. Yang, V. Shrotriya, G. Yang, Y. Yang, *Adv. Funct. Mater.* **2007**, 17, 1636.

- [38] T.H. Kim, J. Hwang, W.S. Hwang, J. Huh, H. Kim, S.H. Kim, J.M. Hong, E.L. Thomas, C. Park, *Adv. Mater.* **2008**, 20, 522.
- [39] S.H. Kim, M.J. Misner, T. Xu, M. Kimura, T.P. Russell, *Adv. Mater.* **2004**, 16, 226.
- [40] L. Yang, X. Li, E. Allahyarov, P.L. Taylor, Q.M. Zhang, L.Zhu, *Polymer* **2013**, 54, 1709.
- [41] B. O. Jun, G. J. Lee, J. G. Kang, S. Kim, J. W. Choi, S. N. Cha, J. I. Sohn, J. E. Jang, *Sci. Rep.* **2015**, 5, 18621.

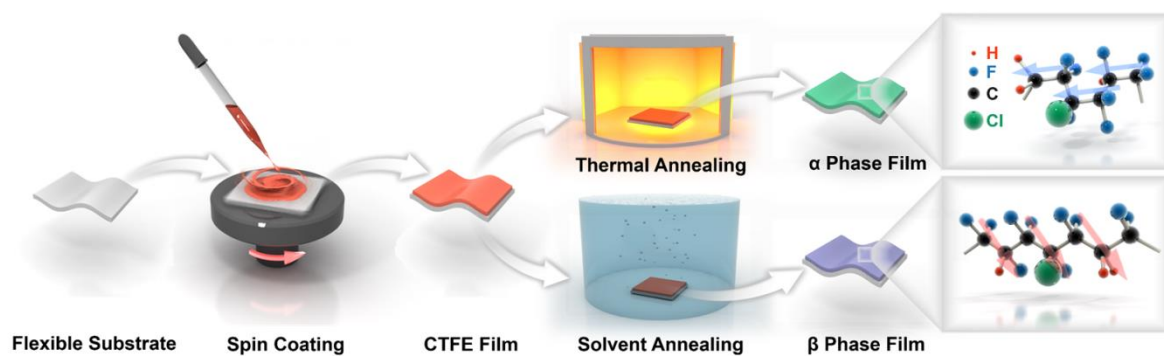


Figure 1. An illustration of the formation of the α and β phases that are formed using thermal and solvent annealing, respectively. Annealing at a temperature below the F-P phase transition, using so-called solvent annealing, forms a β -phase dominant film whereas thermal annealing above the phase transition temperature forms an α -phase dominant film.

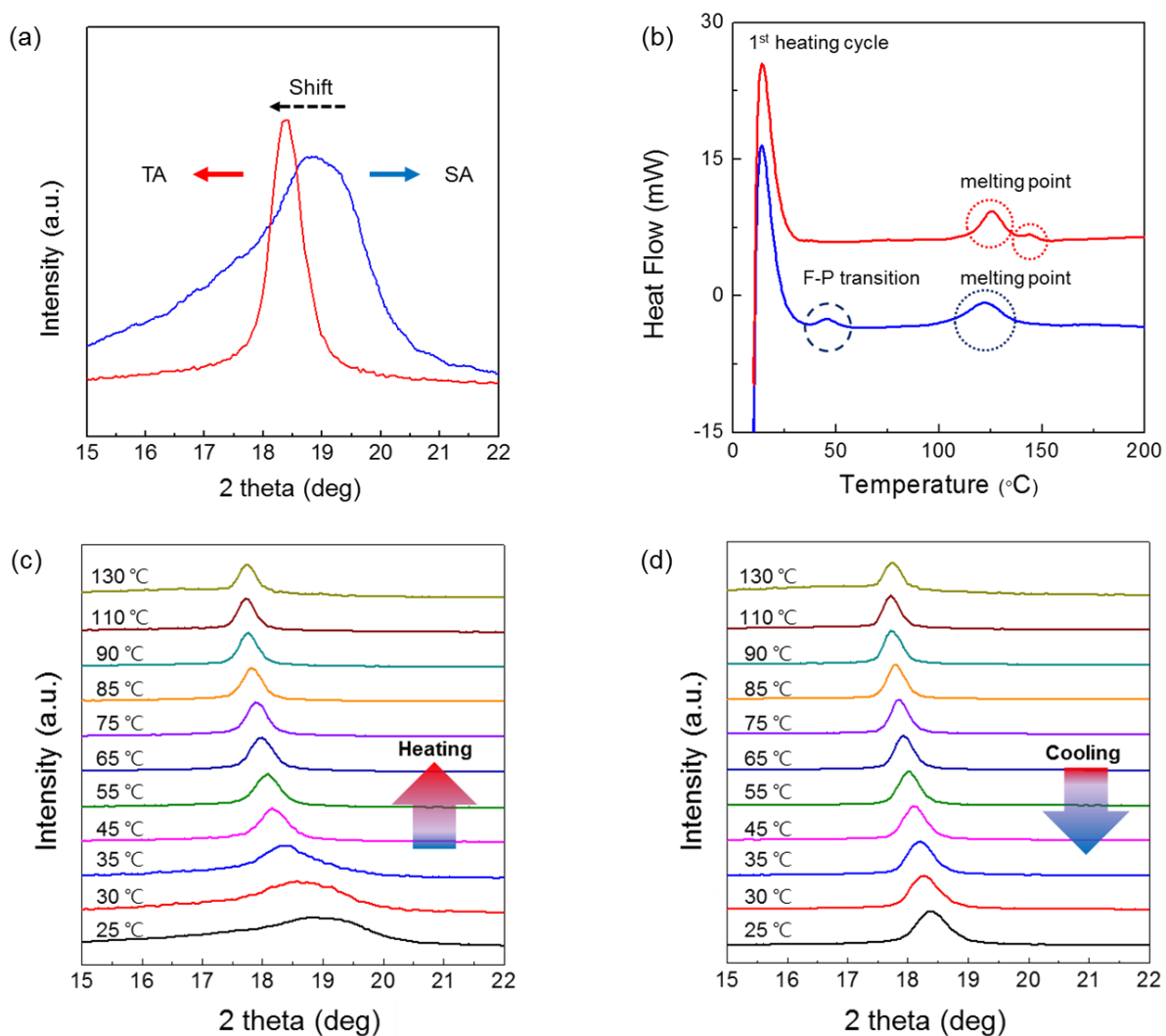


Figure 2. (a) XRD peaks at 25 $^\circ\text{C}$ before heating (Blue) and at 25 $^\circ\text{C}$ after heating and then cooling (Red). (b) First heating cycle of DSC measurement on each SA (Blue) and TA (Red) film. *in-situ* XRD measurements during the (c) heating cycle and (d) cooling cycle.

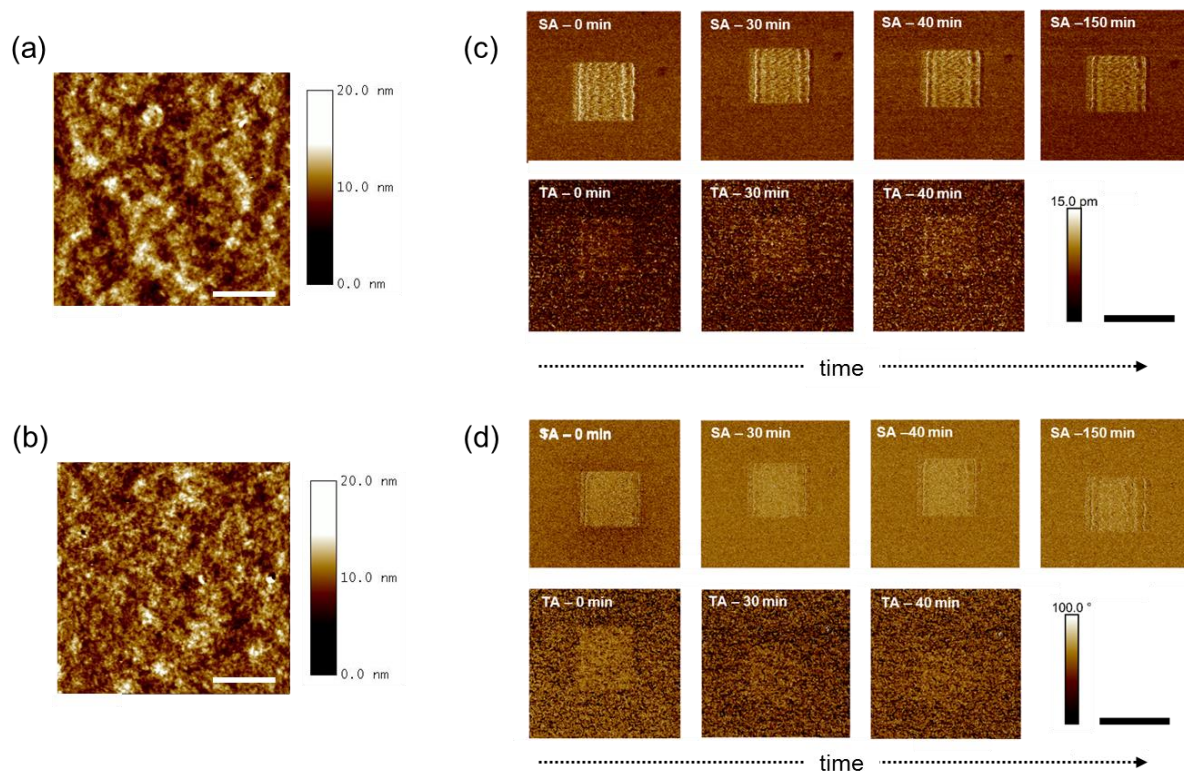


Figure 3. AFM surface images of (a) an SA film and (b) a TA film. (c) PFM amplitude and (d) PFM phase images of the SA film (Top) and TA film (Bottom) (scale bar: 1 μm).

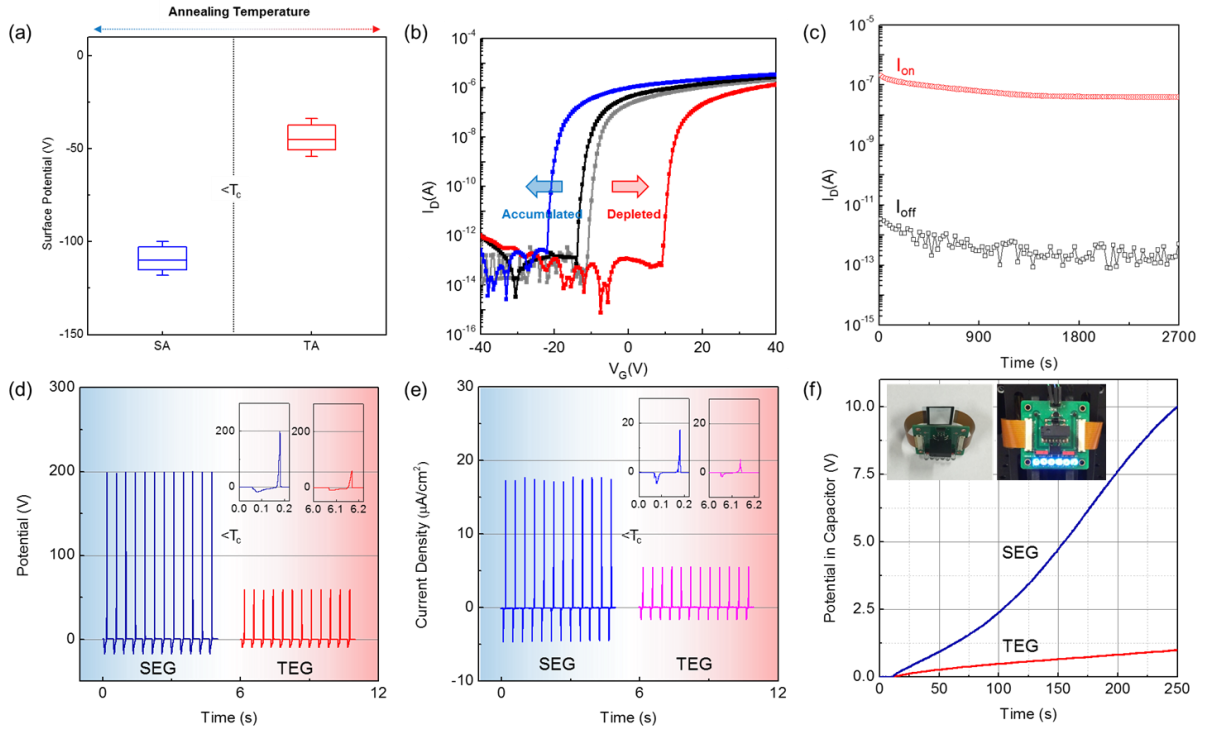


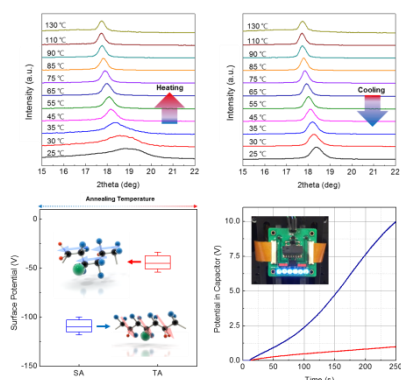
Figure 4. (a) Surface potential measurement of the SA (blue) and TA (red) films. (b) Shift of transfer curve, i.e. threshold voltage (V_{th}), with respect to transfer curve of after deposition of solvent annealed P(VDF-TrFE-CTFE) film (black) as a reference; before deposition of CTFE on IGZO channel (grey), after performing negative poling to the gate electrode (blue), and after performing positive poling to the gate electrode (red). (c) Retention time measurement of SAMD device where red curve indicates on-current and black curve off-current. (d),(e) and (f) show the result of energy harvesting devices that were driven at an input frequency of 3 Hz with a pressure of 2 N cm^{-2} . (d) Potential and (e) current density that were harvested energy by SEG (blue) and TEG (red). (f) Potential charged in the capacitor by SEG (blue) and TEG (red).

The ferroelectric β -phase in a P(VDF-TrFE-CTFE) film is successfully formed using a room temperature solvent annealing process and shows enhanced ferroelectricity compared to a thermally annealed film. Applications in electronics and energy are demonstrated with significantly enhanced device performances for an SA film employed devices compared to a TA film employed due enhanced ferroelectricity of the SA film.

Keyword ferroelectric polymers, ferroelectric phase, paraelectric phase, phase transition, solvent annealing, P(VDF-TrFE-CTFE)

Yuljae Cho^a, Docheon Ahn^a, Jong Bae Park, Sangyeon Pak, Sanghyo Lee, Byoung Ok Jun, John Hong, Su Yong Lee, Jae Eun Jang, Jinpyo Hong, Stephen M. Morris, Jung Inn Sohn*, SeungNam Cha*, and Jong Min Kim

Enhanced ferroelectric property of P(VDF-TrFE-CTFE) film using room temperature crystallization for high performance ferroelectric device applications



Supporting Information

Enhanced ferroelectric property of P(VDF-TrFE-CTFE) film using room temperature crystallization for high performance ferroelectric device applications

Yuljae Cho^a, Docheon Ahn^a, Jong Bae Park, Sangyeon Pak , Sanghyo Lee, Byoung Ok Jun, John Hong, Su Yong Lee, Jae Eun Jang, Jinpyo Hong, Stephen M. Morris, Jung Inn Sohn*, SeungNam Cha*, and Jong Min Kim

*Material Characterization.**1. In-situ XRD measurement.*

High-resolution synchrotron powder x-ray diffraction data of the samples were measured at 9B beamline of PLS-II. The incident x-rays were vertically collimated by a mirror, and monochromatized to the wavelength of 1.1398(1) Å using a double-crystal Si(111) monochromator. After holding at a setpoint of temperature for 10 minutes, *in-situ* XRD measurement was performed.

2. DSC measurement.

SA and TA samples were prepared on copper foil which was then etched by 0.1 M ammonium persulfate. Free standing SA and TA samples were made into powders and delivered to Aluminum pans on a diamond DSC under a helium purge at 50 ml min⁻¹. 3 cycles of DSC analysis were performed using the following conditions: Hold at 10 °C for 2 minutes; Ramp temperature to 250 °C at 200 °C min⁻¹; Hold at 250 °C for 0.5 minute; Cool temperature to 10 °C at 200 °C min⁻¹.

3. Thickness measurement.

The thickness of samples prepared on a silicon substrate was measured by a DEKTAK. For SA films, the film thickness was around 2.1, 1.0, 0.55, 0.16 µm for 10, 5, 4, 2 wt% solution, respectively. The thickness of a TA film was around 2.3, 1.18, 0.6, 0.19 µm for 10, 5, 4, 2 wt% solution, respectively.

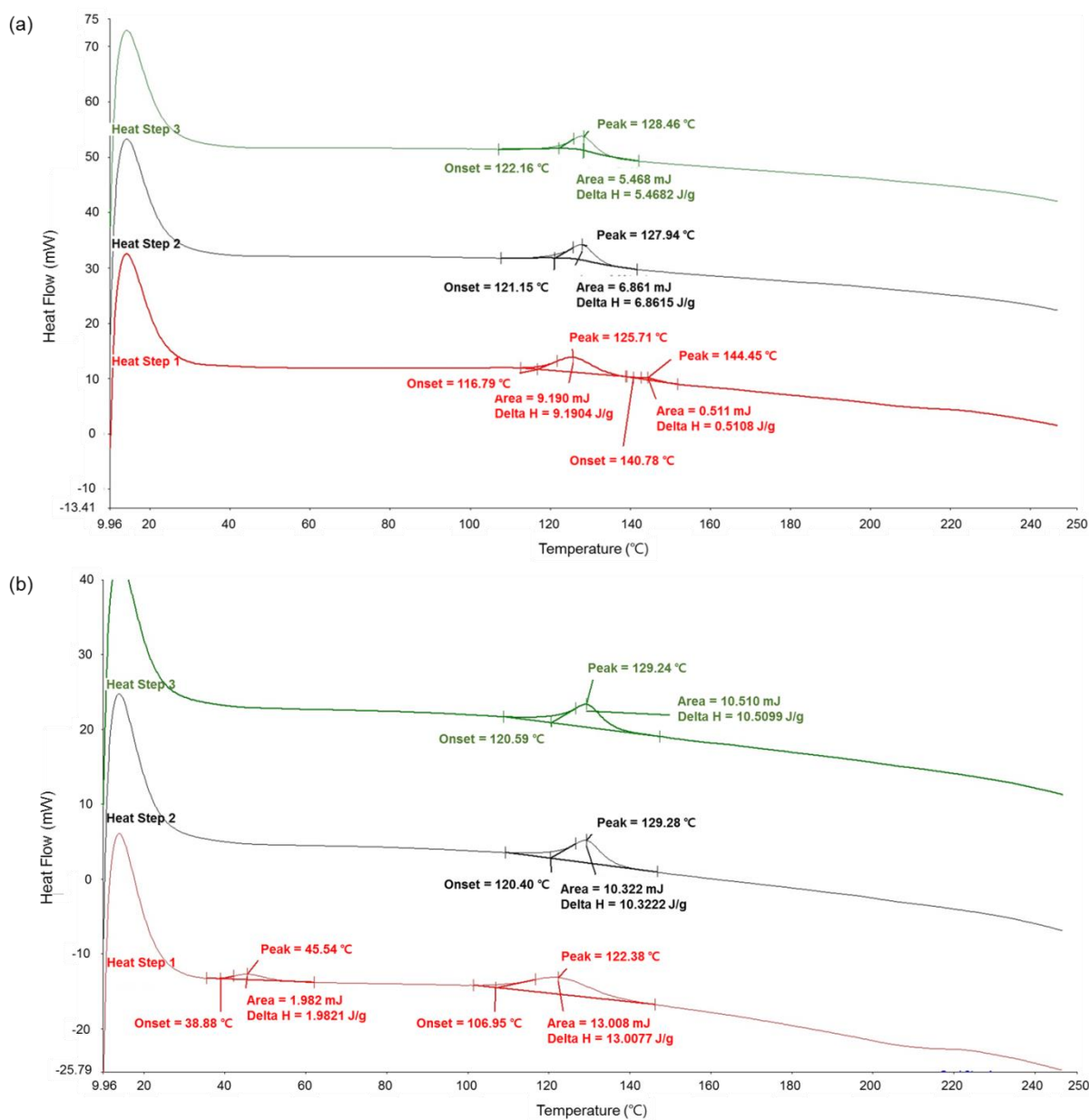
4. PFM measurement.

The PFM of P(VDF-TrFE-CTFE) was conducted with an atomic force microscope (AFM), Multimode 8 (Nanoscope V, Bruker) and the Pt/Ir coated AFM probe (SCM-PIC, Bruker). Local poling of an SA and a TA film was carried out using the tip at 10 V DC bias with a 1 µm scan size at 5 m s⁻¹ scan rate. The applied bias for poling process was relatively lower than the film thickness in order to avoid a deformation of the surface as

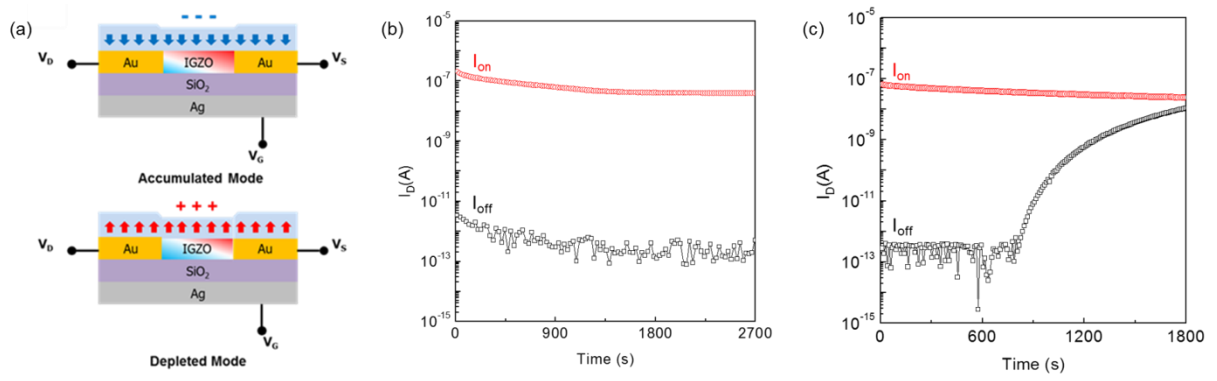
the polymer has a soft and flexible surface. The PFM signals were taken at 2 V AC bias with a frequency of 15 kHz and 2 μm scan size at 5 m s^{-1} scan rate.

Cycle	TA			SA		
	Start/°C	Peak/°C	$\Delta H/J.g^{-1}$	Start/°C	Peak/°C	$\Delta H/J.g^{-1}$
1 st	-	-	-	38.88	45.54	1.982
	116.79	125.71	9.190	106.95	122.38	13.008
	140.78	144.45	0.511	-	-	-
2 nd	121.15	127.94	6.862	120.40	129.28	10.322
3 rd	122.16	128.46	5.468	120.59	129.24	10.510

Supplementary Table 1. The results of a DSC analysis on a TA and an SA film for 3 heating and cooling cycles.



Supplementary Figure S1. DSC graphs of 3 heating and cooling cycles on (a) a TA film and (b) an SA film.



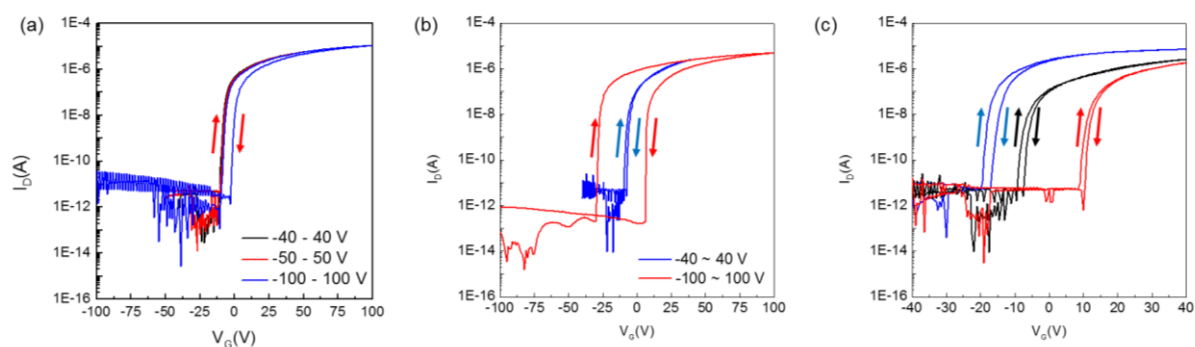
Supplementary Figure S2. (a) Description of Accumulated and Depleted mode of a memory device with respect to the direction of electric dipoles. The comparison of retention time measured with (b) SAMD and (b) TAMD.

Parameters	Value
Vacuum permittivity (ϵ_0)	8.8540E-12
V_{ds} (V)	1.0
Dielectric Constant (ϵ_r)	3.9
Dielectric Thickness (nm)	200
Channel length (L) (μm)	5
Channel width (W) (μm)	8

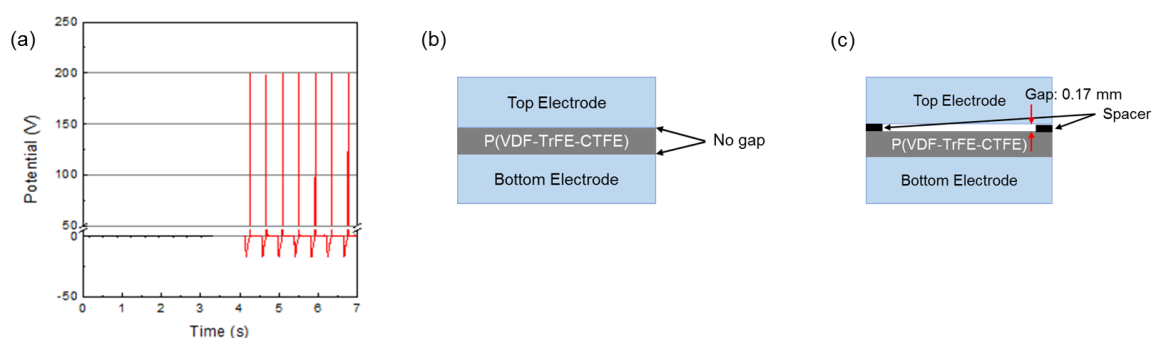
Supplementary Table 2. Device parameters for the ferroelectric memory devices (SAMD) in Figure 4(b).

Sample	Mobility ($\text{cm}^2\text{V}^{-1}\text{S}^{-1}$)	Threshold voltage (V)	Subthreshold swing (Vdec^{-1})
IGZO (grey)	2.9725	-10.7	0.4543
Before poling (black)	2.9656	-13.4	0.3804
Negative poling (blue)	3.0043	-21.6	0.4135
Positive poling (red)	2.7470	9.9	0.4805

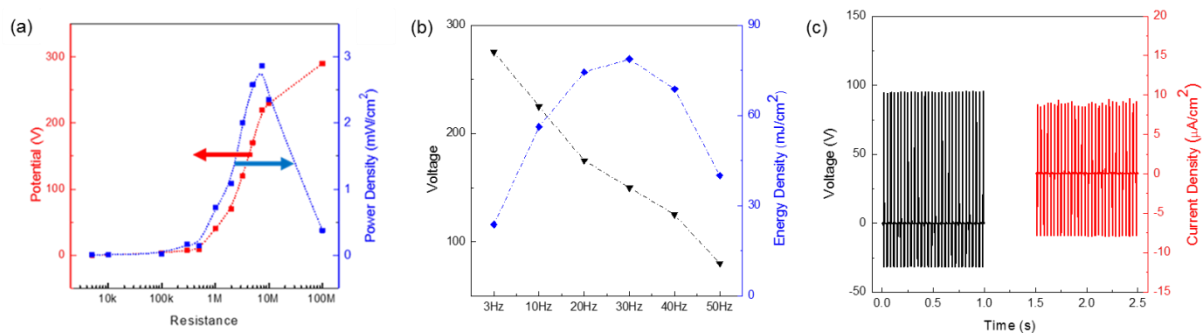
Supplementary Table 3. Characteristics of the ferroelectric memory devices (SAMD) in Figure 4(b).



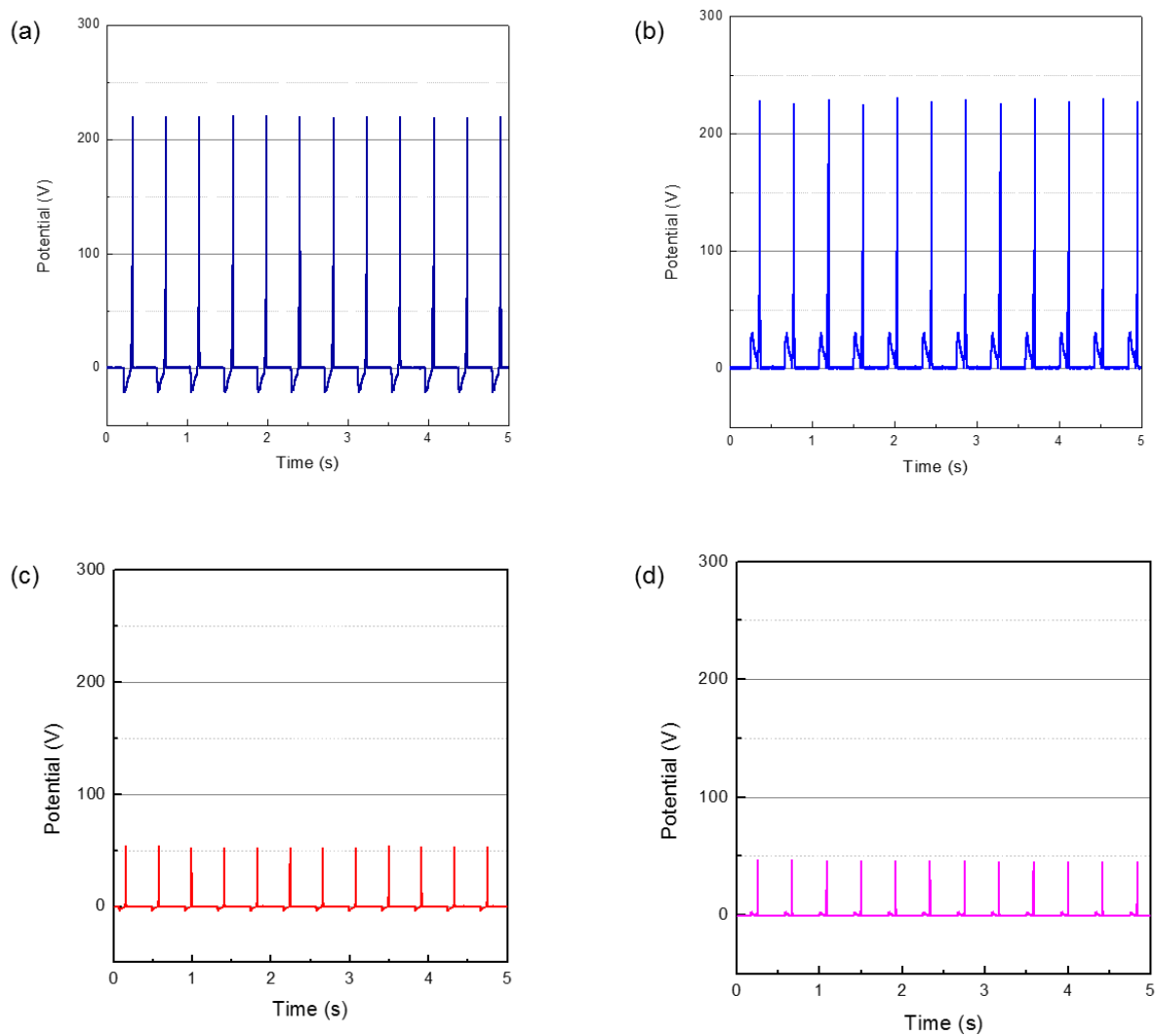
Supplementary Figure S3. (a) Hysteresis effect of IGZO FET with respect to different ranges of the gate voltage sweep. (b) Hysteresis effect of the ferroelectric memory devices (SAMD) with respect to different ranges of the gate voltage sweep. (c) Hysteresis effect of ferroelectric memory devices (SAMD) in the gate voltage sweep range -40 to 40 V.



Supplementary Figure S4. (a) Generated potential from only the piezoelectric effect (black) and the combined piezoelectric and the triboelectric effects (red) of the energy generator (Break on y axis is from 5 to 50 V). Structure of the energy harvesting device (b) without a spacer so as to observe only the piezoelectric effect and (c) with a spacer so that both piezoelectric and triboelectric effects could be recorded.



Supplementary Figure S5. (a) Maximum power transfer measurement by differentiating loads measured at the input frequency 3 Hz. The input frequency was controlled by a pressure stamping machine from 1 to 50 Hz. (b) Voltage and calculated energy density at different input frequencies. (c) Voltage and current density of the SEG driven at 30 Hz input frequency.



Supplementary Figure S6. Voltage output of the SEG (a) before rectifying and (b) after rectifying. Voltage output of TEG (c) before rectifying and (d) after rectifying.